Vietnam Journal of Earth Sciences, 48(4), 609–632, https://doi.org/10.15625/2615-9783/25019

Vietnam Journal of Earth Sciences
https://vjs.ac.vn/index.php/jse



SWAT-based multi-index assessment of meteorological, agricultural, and hydrological drought characteristics in the Mekong River Basin

Anh Nguyen Quoc[1,2], Thi-Thu-Ha Nguyen[1,2], Phong Nguyen Thanh[1,2], Vuong Nguyen Dinh[3,4], Dang Duc Thanh[5], Nguyet-Minh Nguyen[1,2], Duong Tran Anh[1,2,*]

[1]*Laboratory of Environmental Sciences and Climate Change, Institute for Computational Science and Artificial Intelligence, Van Lang University, Ho Chi Minh City, Vietnam*
[2]*Faculty of Environment, Van Lang School of Technology, Van Lang University, Ho Chi Minh City, Vietnam*
[3]*Southern Institute of Water Resources Research, Ho Chi Minh City, Vietnam*
[4]*Vietnam Academy for Water Resources, Hanoi, Vietnam*
[5]*New Zealand Institute for Earth Science, Hamilton, New Zealand*

Received 27 November 2025; Received in revised form 10 April 2026; Accepted 03 August 2026

ABSTRACT

Drought has intensified across the Mekong River Basin (MRB) due to climate variability and increasing human interventions, creating substantial risks for water resources and agriculture. This study applied the SWAT model to simulate hydrological processes and evaluate meteorological, agricultural, and hydrological droughts using the SPI, SSWI, and SRI indices. Model calibration (1982–2001) and validation (2002–2019) at seven hydrological stations produced satisfactory to very good performance, with R^2 values ranging from 0.80 to 0.89 and 0.52 to 0.69, respectively. The model effectively captured seasonal flow dynamics, although uncertainties increased toward downstream regions influenced by reservoir operations and land-use change. Analysis of precipitation and soil moisture revealed strong spatial contrasts among sub-basins: upstream areas exhibited limited infiltration and rapid drainage. At the same time, midstream and downstream regions retained soil moisture longer due to favorable topography and soil characteristics. Multi-decadal drought evaluation reveals several prominent drought periods from 1970 to 2000, consistent with major large-scale climate anomalies. Correlation analysis shows stronger linkages among drought indices at longer accumulation periods, indicating tighter coupling of drought processes under prolonged dry conditions. Overall, integrating SWAT simulations with multi-index drought diagnostics provides a robust framework for characterizing meteorological, agricultural, and hydrological drought dynamics, supporting improved drought monitoring and water resource management in the MRB.

Keywords: Mekong River basin, drought indices, SWAT model.

1. Introduction

Under global climate change, droughts have become increasingly widespread, frequent, intense, and prolonged, particularly in developing countries where adaptive capacity remains limited (Konapala et al., 2020; Loc et al., 2021). As one of the most complex and unpredictable climate extremes, drought has profound economic, social, and environmental impacts worldwide (Duan &

*Corresponding author, Email: duong.trananh@vlu.edu.vn

Mei, 2014; Mishra & Singh, 2010; Wilhite, 2000; Zhang et al., 2022). Prolonged water deficits, often lasting from several months to multiple years, threaten sustainable development and jeopardize livelihood security in vulnerable regions (Konapala et al., 2020; Loc et al., 2021). Although advancements in monitoring and observation technologies have improved drought detection, substantial challenges remain in identifying, classifying, and understanding the mechanisms of drought formation due to the multifaceted nature of drought and the complex interactions among atmospheric, hydrological, and ecological processes (Wilhite, 2000). Typically, drought is classified into three major categories: (1) meteorological drought caused by precipitation deficits, (2) hydrological drought reflected in reduced streamflow and declining surface and groundwater storage, and (3) agricultural drought arising when soil moisture falls below crop water requirements (Dai, 2011; Mishra & Singh, 2010; Sheffield et al., 2004; Van Loon, 2015). These drought types are not independent but interact dynamically, with deficits in one domain often propagating to others and amplifying overall drought severity (Guo et al., 2020; Van Loon & Van Lanen, 2012).

In a rapidly changing environment, drought can no longer be regarded as a purely natural hazard, as human activities increasingly modify its characteristics and the ways societies respond to it (Q. Tang, 2020; Van Loon et al., 2016). Climate change and anthropogenic interventions exert both direct and indirect impacts on drought formation and progression. Direct influences include irrigation, reservoir operations, and changes in snowmelt dynamics, whereas indirect impacts arise from landscape modification, deforestation, and population growth (Guo et al., 2017; He et al., 2017; Qiu, 2010).

These combined natural and human-driven pressures are clearly reflected in the Mekong River Basin (MRB), one of Asia's most significant transboundary river systems, which sustains regional agriculture and water resources. Over the past two decades, the MRB has experienced multiple severe droughts, and future projections indicate increasingly intense and persistent events (Son et al., 2012; Thilakarathne & Sridhar, 2017). Historical records document the magnitude of these impacts: the 1990-1992 drought resulted in approximately USD 210 million in rice production losses in Thailand (Pandey et al., 2007), the 1997-1998 drought caused about USD 400 million in agricultural damages in Vietnam (Nguyen & Shaw, 2011), and the 2004–2005 drought affected more than 104,000 hectares of rice and disrupted livelihoods across 14 Cambodian provinces (Cosslett & Cosslett, 2017). The basin-wide impacts of the 2015–2016 drought further illustrate the MRB's growing vulnerability to extreme hydroclimatic stressors (Keovilignavong et al., 2023). While these events have often been attributed to climatic anomalies, several studies also highlight that upstream hydrological alterations, including reservoir regulation and dam construction, may intensify drought impacts (Lu et al., 2014; Mekong River Commission, 2005).

Many studies have examined drought under climate change across river basins worldwide, providing an important foundation for understanding conditions in the MRB. In the Salt Creek Basin (USA), D. Wang et al. (2011) reported an increasing trend in future drought frequency across meteorological, agricultural, and hydrological dimensions by employing RCMs and integrating climate outputs into an agro-hydrological model to simulate Standardized Precipitation Index (SPI), Standardized Soil Water Index (SSWI), and Standardized Runoff Index (SRI). Similar patterns have been documented in China (Leng et al., 2015) and the Lerma Basin in Spain (Gunten et al., 2016). In the Karkheh

Basin, Kamali et al. (2017) applied the Soil and Water Assessment Tool (SWAT) model combined with five bias-corrected GCMs to compute SPI, SRI, and SSWI for constructing the Drought Hazard Index (DHI), indicating a higher likelihood of severe and extreme droughts in the future, particularly hydrological and agricultural droughts. Sam et al. (2019) further demonstrated an increase in the frequency of extreme droughts in the Srepok River Basin using SWAT and multiple drought indices. Collectively, these studies highlight the essential role of hydrological models in drought simulation and monitoring and emphasize the importance of selecting appropriate drought indices to accurately characterize dry conditions.

In the context of the MRB, meteorological indices such as SPI and SPEI (Dong et al., 2022; Lee & Dang, 2019; Y. Li et al., 2021), agricultural indices such as SSI (Kang et al., 2021), and multivariate indices such as MSDI (Kang et al., 2021) have been widely applied, reflecting substantial spatial and temporal variability in drought conditions across the basin. Recent studies have particularly highlighted prolonged dry periods, including the 1991-94 drought and the widespread drought conditions in 2015–2016 within the MRB (Dong et al., 2022; Kang et al., 2021).

Most existing drought assessments in the MRB have primarily focused on individual drought types or local-scale analyses, thereby limiting a comprehensive understanding of basin-wide drought characteristics and the interactions among meteorological, agricultural, and hydrological droughts. A framework integrating multiple drought indicators is therefore required to better characterize their temporal evolution and spatial variability across the basin.

Accordingly, this study aims to address three specific questions: (1) whether the SWAT model can adequately reproduce the hydrological behavior of the Mekong River Basin; (2) what are the temporal characteristics and long-term evolution of meteorological, agricultural, and hydrological droughts represented by the SPI, SSWI, and SRI; and (3) how do climatic and physiographic factors affect drought characteristics and soil moisture variability across different regions of the basin?

To address these questions, the SWAT model was calibrated and validated for the period 1982–2019. Subsequently, the SPI, SSWI, and SRI were calculated at accumulation periods of 3, 6, and 12 months. The temporal evolution of drought conditions, relationships among drought indices, precipitation-soil moisture interactions, and the spatial variability of soil moisture were further investigated.

The findings of this study provide a comprehensive assessment of drought characteristics across the MRB and offer insights to support drought monitoring and sustainable water resources management in this transboundary basin.

2. Methodology

2.1. Study area

The Mekong River extends approximately 4,800 km, ranking as the 12th-longest river in the world. Its basin covers about 795,000 km^2, placing it 21st globally in area, and generates an average annual runoff of approximately 475,000 million m^3, ranking it 8th worldwide. The basin is shared by six countries, including China (21%), Myanmar (3%), Lao PDR (25%), Thailand (23%), Cambodia (20%), and Vietnam (8%). From a hydrological and political perspective, the basin is divided into two main sub-regions: the Upper Mekong River Basin (UMRB) in China, known as the Lancang River, and the Lower Mekong River Basin (LMRB), which extends from the China-Laos border to the East Sea in Vietnam (Ogston et al., 2017). The Upper Basin has a

river length of approximately 2,139 km, while the Lower Basin spans about 2,770 km across five downstream countries (Tang et al., 2019).

Climatic conditions differ markedly between the UMRB and LMRB. A temperate climate influences the Upper Basin. In contrast, the Lower Basin is governed by a tropical monsoon regime with distinct wet (May-October) and dry (November-April) seasons (Kang et al., 2021; Le et al., 2024). Approximately 80% of annual precipitation occurs during the Southwest Monsoon, resulting in strong hydrological seasonality (Le et al., 2024). In the Lower Basin, the mean annual rainfall ranges from 1,000 to 3,000 mm, with substantial spatial and temporal variability (Le et al., 2024; Tang et al., 2019). Recent decades have also been marked by severe drought events, posing significant challenges to water resources, agriculture, and food security (Kang et al., 2021).

At the same time, rapid hydropower development has intensified river regulation. Seven mainstream dams are under construction in China, and 133 projects have been proposed in the Lower Mekong Basin, including 11 on the mainstream (Kondolf et al., 2014). Existing reservoirs in the Upper Basin have active storage capacities ranging from 120 to 12,300 million m^3. In comparison, the proposed mainstream dams in the Lower Basin are expected to have storage capacities of 115 to 1,450 million m^3. Differences in operational regimes, seasonal to annual regulation upstream, and daily operation downstream have significantly modified flow regimes, sediment transport, and sediment delivery to the Mekong Delta (Yoshida et al., 2020). The combined effects of climatic variability and dam regulation are therefore increasing pressure on basin-wide hydrological stability and delta sustainability.

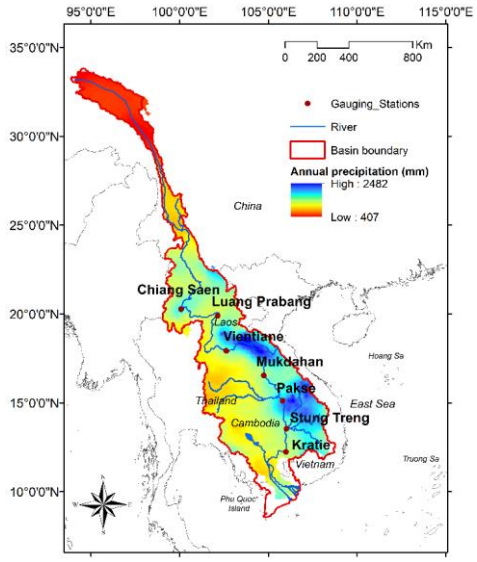


Figure 1. Location of the Mekong River Basin and distribution of monitoring stations

2.2. SWAT hydrological model

The SWAT model is a physically based, semi-distributed model developed by the Agricultural Research Service of the U.S. Department of Agriculture (Arnold et al., 1998; C. Li & Fang, 2021). It has been widely applied for hydrological simulations at the watershed scale (Arnold et al., 1998; Ghaith & Li, 2020; Inseeyong et al., 2024). The required data includes daily rainfall and temperature, land use, soil types and properties, a digital elevation model (DEM), and hydrological information. Based on these datasets, the basin is delineated into multiple sub-basins, which are further partitioned into Hydrological Response Units (HRUs) defined by unique combinations of soil type, land use, and slope (Inseeyong et al., 2024). This hierarchical structure enables the model to represent spatial heterogeneity across the watershed. SWAT simulates the overall water balance for each HRU, with outputs generated at daily, monthly, and annual time steps (Mohammed et al., 2018). In this study, the MRB was divided into 87 sub-basins, totaling 983 HRUs. The water balance equation is expressed as follows (Eq. 1):

$$PREC = ET + GWQ + SURQ + Infitration + \Delta SW \quad (1)$$

Where $PREC$ denotes mean annual precipitation (mm); ET represents actual evapotranspiration (mm); GWQ refers to groundwater contribution to streamflow (mm); and ΔSW is the change in soil water content between the end and beginning of the year (mm).

2.3. Data collection

The datasets used in this study, together with their sources and spatial resolutions, are summarized in Table 1. Most of the gridded data were available at a spatial resolution of 0.25 × 0.25°. Land use/land cover data for the MRB were obtained from the Global Land Cover Characteristics 2000 (https://forobs.jrc.ec.europa.eu/glc2000). Soil data were acquired from the Food and Agriculture Organization (FAO) of the United Nations (https://www.fao.org/home/en/), while the DEM was derived from the Shuttle Radar Topography Mission (https://www.earthdata.nasa.gov/data/instruments/srtm) (Table 1). These global datasets are widely employed in basin-scale hydrological modeling and have been extensively evaluated in previous studies (e.g., He et al., 2021; Nguyen et al., 2023; Tran et al., 2023; Vu et al., 2015a). The use of standardized and spatially consistent products enhances methodological coherence across the transboundary basin and supports the robustness and reproducibility of SWAT-based simulations in the MRB.

Table 1. Data inputs and sources in the SWAT model

Data type	Source	Resolution	Year/Period
Land use/Land cover	Global Land Cover Characteristics (GLCC)	0.25 × 0.25°	2000
Soil map	Food and Agriculture Organization (FAO)	0.25 × 0.25°	2003
DEM	Shuttle Radar Topography Mission (SRTM)	0.25 × 0.25°	2011
Daily precipitation	Climate Prediction Center (CPC)	0.25 × 0.25°	1970–2019
Daily temperature	Climate Prediction Center (CPC)	0.25 × 0.25°	1970–2019
Daily discharge	Mekong River Commission (MRC)	-	1970–2019

Meteorological inputs, including daily precipitation and temperature, were obtained from the Climate Prediction Center (CPC) for the period 1970–2019 (https://www.cpc.ncep.noaa.gov/) (Fig. 2). The CPC dataset has been extensively used in hydrological and climate assessments within the MRB, supporting its suitability for basin-scale modeling applications (Duc Dang et al., 2020; Lauri et al., 2014; Vu & Mishra, 2016).

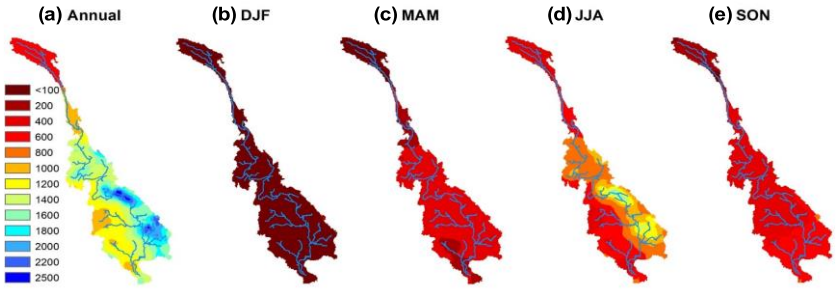


Figure 2. The total annual and seasonal precipitation average over the Mekong River basin

Observed streamflow data for model calibration and validation were obtained from the Mekong River Commission (MRC) (https://www.mrcmekong.org/) at seven key hydrological stations along the mainstream, namely Chiang Saen, Luang Prabang,

Vientiane, Nakhon Phanom, Mukdahan, Pakse, Stung Treng, and Kratie, covering the period 1970–2019.

2.4. Model calibration and validation

The model was calibrated using monthly streamflow data from seven key stations for the period 1982–2001 and validated for the period 2002–2019. Automatic calibration and validation were performed using the Sequential Uncertainty Fitting algorithm version 2 (SUFI-2) (Abbaspour et al., 2007) in the SWAT-CUP tool package (Abbaspour, 2013; Tuo et al., 2016). The one-at-a-time procedure of SWAT-CUP initially performed a sensitivity analysis to identify the most influential parameters affecting model performance (Li et al., 2021). This procedure tests model sensitivity by varying one parameter while keeping all others constant (Tuo et al., 2016).

Fifteen parameters were determined to calibrate the model based on a literature review of previous MRB studies by Kang & Sridhar (2021) and Kang et al. (021). The sensitivity of the parameters was considered by the p-value (p-value ≤ 0.05). The most sensitive parameters were eight parameters, including the effective hydraulic conductivity in main channel alluvium (V_CH_K2), Manning "n" value for the main channel (V_CH_N2), Saturated hydraulic conductivity (R_SOL_K), Groundwater delay (V_GW_REVAP), Soil evaporation compensation factor (V_ESCO), SCS runoff curve number (R_CN2), Baseflow alpha factor (V_ALPHA_BF), and Groundwater delay time (V_GW_DELAY) (Table 2).

Table 2. Parameters used in the SWAT model calibration

Parameters	Description and units	Input file	Range	Calibrated values
V_CH_K2	Effective hydraulic conductivity in main channel alluvium (mm/h)	.rte[a]	-0.01–500	64.991
V_CH_N2	Manning "n" value for the main channel	.rte[b]	-0.01–0.3	0.080
R_SOL_K	Saturated hydraulic conductivity	.sol[c]	0.013–0.038	0.016
V_GW_REVAP	Groundwater delay (days)	.gw	0.16–0.27	0.258
V_ESCO	Soil evaporation compensation factor	.bsn	0.5–0.9	0.576
R_CN2	SCS runoff curve number	.mgt	-0.05–0.15	0.116
V_ALPHA_BF	Baseflow alpha factor (days)	.gw	0.06–0.7	0.143
V_GW_DELAY	Groundwater delay time (days)	.gw	0–500	435

Note: The extension (e.g., rte) refers to the SWAT input file where the parameter occurs. [b] The qualifier (V) refers to the substitution of a parameter by a value from the given range. [c] The qualifier (R) refers to the relative change in parameter, where the value from the SWAT database is multiplied by 1 plus a factor in the given range

The model performance was evaluated using several statistical indicators, including the coefficient of determination (R^2), root mean square error (RMSE), Kling-Gupta efficiency (KGE), and percent bias (PBIAS). The detailed formulations of these metrics are described in previous studies by Knoben et al. (2019), Mccuen et al. (2006), and Moriasi et al. (2007, 2012).

These metrics provide complementary insights into model reliability by capturing different aspects of model performance. Specifically, R^2 reflects the strength of the linear relationship between observed and simulated streamflow, while RMSE quantifies the magnitude of prediction errors, with lower values indicating better performance. KGE offers an integrated assessment by simultaneously accounting for correlation, variability, and bias between simulated and observed values; values closer to 1 indicate better agreement. Meanwhile, PBIAS evaluates the average tendency of simulated values to over- or underestimate observations;

positive values indicate underestimation, and negative values indicate overestimation.

2.5. Drought indices calculation

To characterize meteorological, agricultural, and hydrological drought conditions across the basin, three standardized indices were employed: the Standardized Precipitation Index (SPI), the Standardized Soil Water Index (SSWI), and the Standardized Runoff Index (SRI). A common accumulation period of 6 months was adopted to ensure consistency in drought assessment, while additional analyses at 3- and 12-month time scales were performed to examine the effects of temporal aggregation on drought characteristics. As reported by Vu et al. (2018), shorter accumulation periods emphasize short-term variability, whereas longer accumulation periods smooth temporal fluctuations and better represent persistent drought conditions.

SPI was derived from precipitation data obtained from the CPC dataset (Vu et al., 2017), whereas SSWI and SRI were calculated from soil moisture and streamflow simulated by the SWAT model, respectively (Leng et al., 2015; Shukla & Wood, 2008; Vu et al., 2015b). For SSWI, soil moisture was represented by the total profile soil water content (SOL_SW), which integrates water storage across all soil layers. Following previous studies (Leng et al., 2015; Shukla & Wood, 2008; Vu et al., 2015b), the accumulated series of precipitation, soil moisture, and streamflow were fitted using the Gamma distribution and subsequently transformed into a standard normal distribution to obtain SPI, SSWI, and SRI (Eq. 2).

$$g(x) = \frac{1}{\beta^{\alpha}\Gamma(\alpha)} x^{\alpha-1} e^{-x/\beta}, \text{ for x > 0} \quad (2)$$

In Eq. (2), α and β denote the shape and scale parameters of the Gamma distribution, respectively, while x represents the accumulated value of the corresponding variable, namely precipitation for SPI, soil water content for SSWI, and streamflow for SRI. The Gamma function, $\Gamma(\alpha)$, is expressed in integral form as follows:

$$\Gamma(\alpha) = \int_0^{\infty} y^{\alpha-1} e^{-y} dy \quad (3)$$

Once the probability density function is defined, the cumulative probability is calculated using Eq. (4), representing the probability of observing a given value of the corresponding variable (precipitation, soil water content, or streamflow) at a specified accumulation period. The cumulative probability is then transformed into a standard normal distribution to obtain SPI, SSWI, and SRI.

$$G(x) = \int_0^{\infty} g(x) dx \quad (4)$$

The Gamma function is not defined at $x = 0$, which may occasionally occur in hydro-meteorological variables. Therefore, the cumulative probability $H(x)$ of observing a given quantity of the respective hydro-meteorological variable (i.e., precipitation, soil moisture, or streamflow) is calculated by incorporating the probability of zero values as follows:

$$H(x) = q + (1 - q)G(x) \quad (5)$$

where q is the probability of zero values and $G(x)$ is the cumulative probability derived from the Gamma distribution.

Subsequently, the standardized indices (SPI, SSWI, and SRI) are determined by transforming the cumulative probability $H(x)$ into a standardized normal distribution with a mean of zero ($\mu = 0$) and a standard deviation of one ($\sigma = 1$). This is achieved by taking the inverse of the standard normal cumulative distribution function at the corresponding probability $H(x)$. This equiprobability transformation process is uniformly applied to all three variables, ensuring that SPI, SSWI, and SRI are directly comparable across different spatial and temporal scales. The resulting standardized values denote the severity of meteorological, agricultural, and hydrological droughts, respectively.

Drought characteristics were assessed using three indicators: (i) the number of

drought events, (ii) drought frequency, defined as the proportion of months with index values below -1 relative to the total study period, and (iii) drought severity, calculated as the cumulative sum of all index values below -1.

2.6. ENSO-drought indices relationship

To examine the influence of ENSO on drought variability, Pearson correlation coefficients (r) were calculated between ENSO indicators and drought indices across the 87 sub-basins, and the spatial distribution of correlations was mapped using GIS. Higher absolute values of r indicate stronger linear associations.

The ENSO signal was represented by the Oceanic Niño Index (ONI) averaged over December-January-February (DJF), corresponding to the typical peak phase of ENSO events (Rasmusson & Carpenter, 1982). Previous investigations have shown that precipitation in the LMRB responds to ENSO variability with a delay of about three months (Räsänen et al., 2016; Räsänen & Kummu, 2013). Accordingly, meteorological drought responses were analyzed by correlating DJF ONI with SPI during March-April-May (MAM). Because soil moisture and river discharge do not respond immediately to precipitation anomalies, a 1-month delay relative to SPI was applied when analyzing agricultural and hydrological drought conditions. This lag assumption follows Xue et al. (2011), who reported a lag of approximately 1 month between rainfall and river discharge in the MRB. Therefore, SSWI and SRI during April-May-June (AMJ) were used to represent the delayed impacts of ENSO-related precipitation anomalies.

3. Results and discussion

3.1. Hydrological model results

Model performance was evaluated by comparing the SWAT-simulated streamflow with observed discharge following the approach of Grayson et al. (1992). The results for daily mean streamflow (Table 3) show strong agreement between simulations and observations and meet the performance criteria recommended by Moriasi et al. (2007). During the calibration period (1982–2001), R^2 values ranged from 0.80 to 0.89 and KGE from 0.70 to 0.90, indicating that the model effectively reproduced the correlation, variability, and mean behavior of observed streamflow. RMSE values ranged from 903 m^3/s at Chiang Saen to 5996 m^3/s at Stung Treng, reflecting the increasing discharge magnitude and hydrological complexity toward downstream stations. PBIAS values were generally within acceptable limits, suggesting that the basin-scale water balance was reasonably captured.

Table 3. Daily calibration and validation at seven main gauging stations in the Mekong River Basin

Stations	Calibration (1982–2001)				Validation (2002–2019)			
	R^2	RMSE	KGE	PBIAS	R^2	RMSE	KGE	PBIAS
Chiang Saen	0.82	903	0.90	-0.92	0.54	1199	0.72	2.57
Luang Prabang	0.88	1294	0.87	-8.12	0.63	1838	0.79	1.21
Vientiane	0.87	1687	0.82	-12.33	0.65	2319	0.78	-3.52
Mukdahan	0.89	2454	0.88	4.60	0.69	4861	0.65	24.66
Pakse	0.86	3642	0.89	-7.88	0.74	5287	0.84	3.54
Stung Treng	0.85	5996	0.70	15.12	0.71	6975	0.73	19.09
Kratie	0.82	5548	0.86	-2.91	0.65	7941	0.80	5.60

During the validation period (2002–2019), model performance remained satisfactory, with R^2 values ranging from 0.54 to 0.74 and KGE values from 0.65 to 0.84. RMSE increased at some downstream stations, particularly at Kratie (7941 m^3/s), likely reflecting greater hydrological variability and potential influences of hydropower

development and land-use changes. PBIAS values indicate moderate bias at several stations but remain within acceptable ranges.

Overall, model performance ranged from satisfactory to very good during both calibration and validation periods. According to the studies by Abou Rafee et al. (2019) and Wang et al. (2018), simulations are considered acceptable when R^2 and NSE exceed 0.5, which is satisfied at all stations. Despite the inherent complexity and temporal variability of hydrological processes (Gassman et al., 2014; Mukundan et al., 2010), while the SWAT model demonstrates sufficiently robust performance for applications in the MRB (Mccuen et al., 2006; Moriasi et al., 2007, 2012).

Comparisons of simulated and observed monthly discharge (Fig. 3) show that the SWAT model reproduces the characteristic monsoon-driven seasonal cycle of the MRB. Slight reductions in model accuracy during the validation period are likely related to intensified human interventions in the basin, including reservoir regulation and irrigation expansion, which have modified the natural hydrological regime since the early 2000s (Wang et al., 2016; Wu et al., 2019; Zhao et al., 2013). Despite these uncertainties, the model successfully captures the basin's main hydrological dynamics and provides a reliable representation of streamflow variability for the subsequent drought analysis.

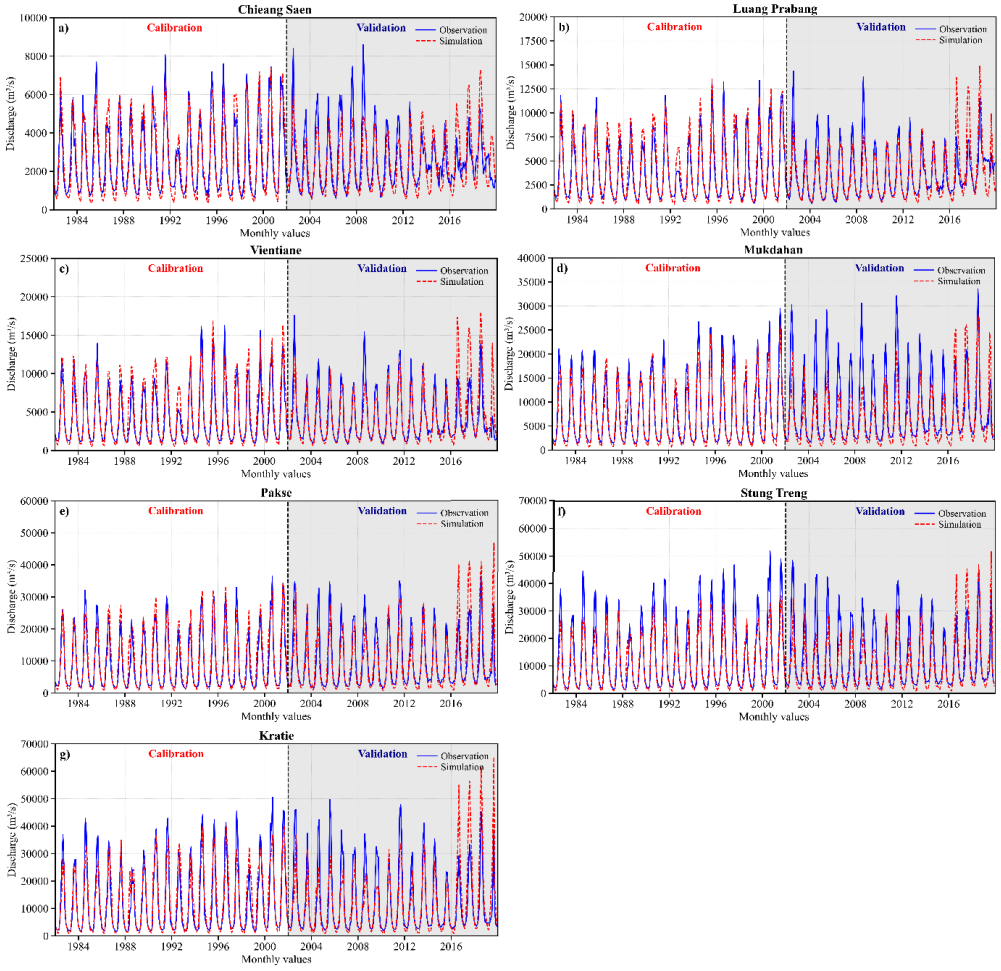


Figure 3. Comparison between observed and simulated monthly discharge at the main gauging station

Scatter plots comparing simulated and observed daily discharge (Fig. 4) indicate a consistent relationship between modeled and measured flows across the basin, with R^2 values ranging from 0.70 to 0.77. Box plot comparisons (Fig. 5) further demonstrate that the model captures the central tendency of daily discharge distributions at most stations. However, simulated flows exhibit slightly wider variability ranges, particularly at downstream locations. Such discrepancies are commonly reported in large river basins. They are often associated with uncertainties in gridded precipitation inputs, spatial rainfall heterogeneity, and structural limitations of semi-distributed models in representing floodplain storage and channel routing processes (Fuka et al., 2014; Räsänen et al., 2017; Zhang et al., 2007). Although dams have been widely acknowledged (Binh et al., 2020; Soukhaphon et al., 2021) to play a substantial role in modulating streamflow regimes across the Mekong River Basin, they were not incorporated in this study due to the lack of reservoir operation data, which introduces additional uncertainty into the simulated streamflow.

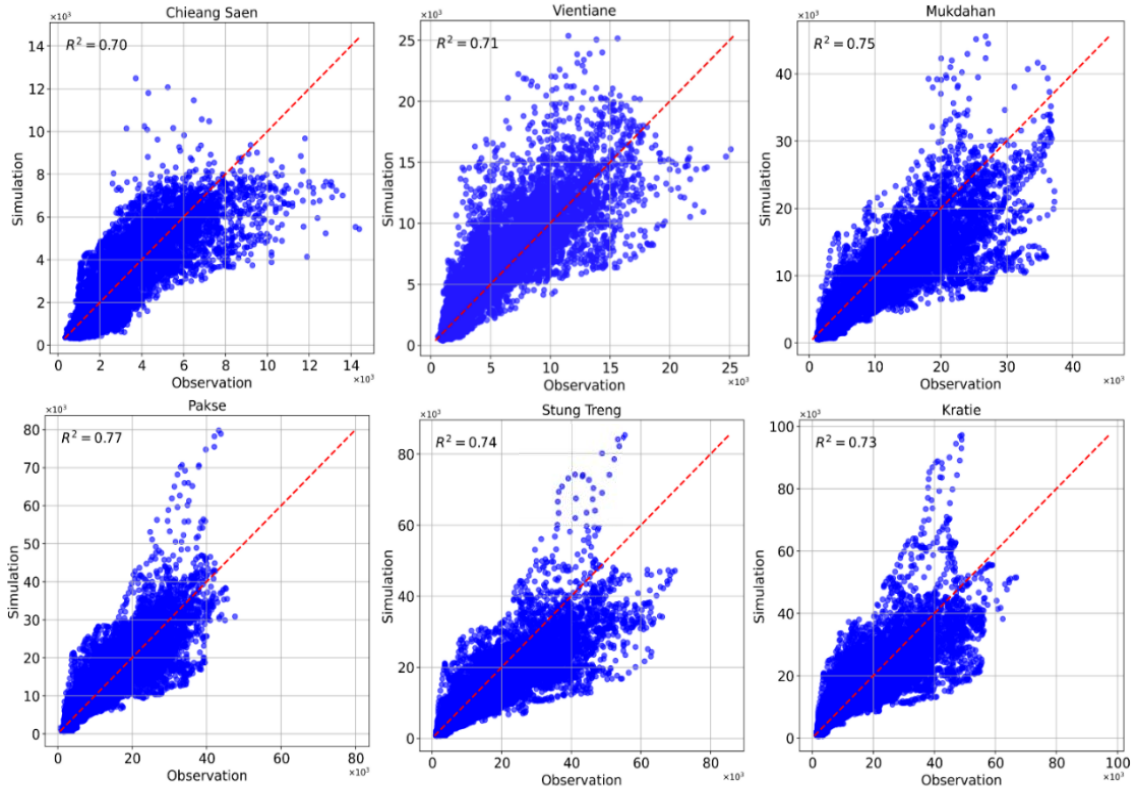


Figure 4. Scatter plots comparing simulated and observed daily discharge at main gauging stations in the Mekong River Basin

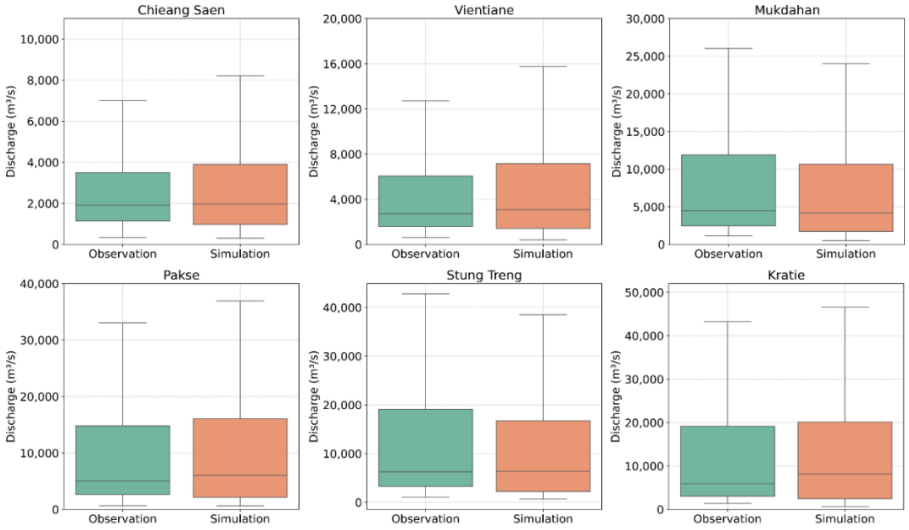


Figure 5. Box plots comparing simulated and observed daily discharge at main gauging stations in the Mekong River Basin

3.2. Dynamics of precipitation and soil moisture across the Mekong Basin

Figure 6 illustrates the relationship between monthly precipitation and soil water content across six representative sub-basins of the MRB, including UMRB, MMB-1, MMB-2, Chi-Mun, 3S, and LMRB, for the drought year 1992. Soil moisture generally follows the seasonal rainfall cycle, decreasing during the dry season (January-April) and increasing markedly as precipitation intensifies during the wet season (May-October). A noticeable seasonal lag between precipitation peaks and soil moisture response can be observed across most sub-basins, reflecting the integrative role of soil moisture as a storage variable within the land surface system. This seasonal pattern reflects the strong influence of the monsoon climate on hydrological processes in tropical river basins (Seneviratne et al., 2010).

Despite the overall seasonal coherence, clear spatial contrasts emerge among the sub-basins. In upstream areas such as UMRB and MMB-1, soil moisture increases more slowly relative to rainfall. This response can be attributed to steep terrain, shallow soils, and limited infiltration capacity, which reduce soil water storage and promote rapid surface runoff generation (Beven & Kirkby, 1979; Western et al., 2002). In contrast, the midstream and downstream regions (MMB-2, Chi-Mun, and LMRB) exhibit higher and more persistent soil moisture levels following rainfall peaks. These areas are characterized by gentler slopes and finer-textured, clay-rich soils that enhance water-holding capacity and slow drainage processes (Mekong River Commission, 2010; Saxton & Rawls, 2006).

The 3S sub-basin exhibits a distinct hydrological response. Although rainfall amounts are relatively high, soil moisture increases more gradually and remains comparatively lower than in other regions. This pattern is consistent with the dominance of sandy, highly permeable soils in the 3S basin, which facilitateapid infiltration and drainage, thereby limiting soil water retention even during periods of heavy rainfall (Trang et al., 2017). Similar responses have been documented in coarse-textured catchments across Southeast Asia.

The seasonal offset between rainfall and soil moisture responses highlights soil moisture as a storage component that integrates

precipitation inputs over time. In monsoon-dominated basins such as the MRB, precipitation first infiltrates into the soil and contributes to soil water storage before gradually being redistributed through evapotranspiration, runoff generation, and percolation. Consequently, soil moisture responds more gradually than precipitation and exhibits a delayed seasonal peak. This storage-controlled behavior plays an important role in regulating soil moisture dynamics and drought development across the basin.

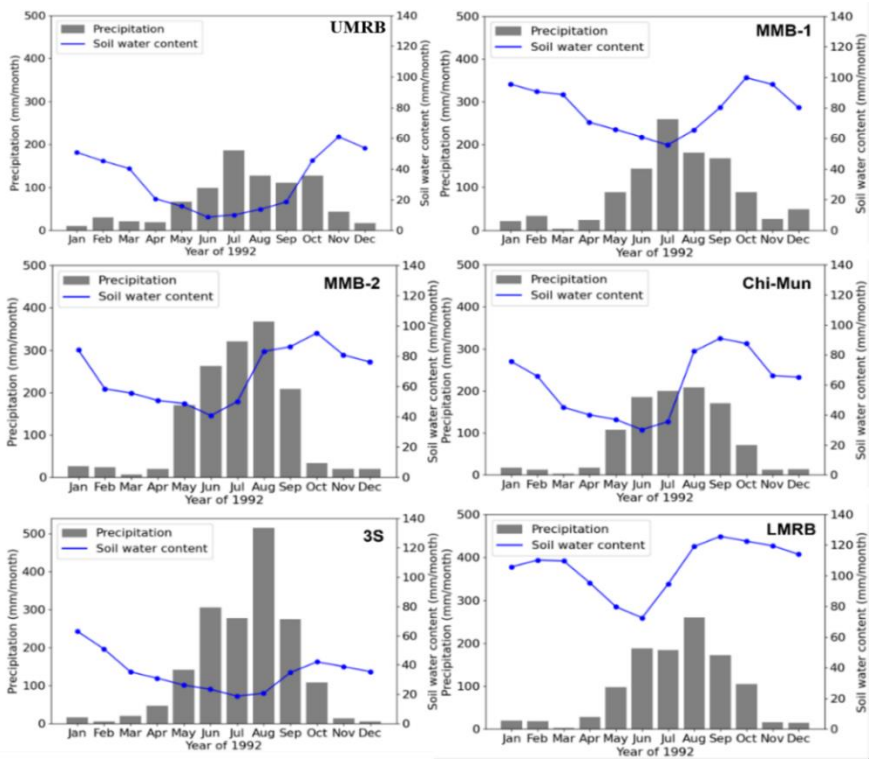


Figure 6. The relationship between precipitation and soil water content in the Mekong River Basin in 1992

3.3. Influence of topography and monsoon climate on hydrological characteristics

Figure 7 illustrates the longitudinal variation in elevation and precipitation across the sub-basins of the MRB. Elevation declines sharply from the steep, mountainous headwaters, where elevations exceed 4000 m, toward the midstream and downstream regions, characterized by low-lying, increasingly flat terrain. This strong topographic gradient is typical of large transboundary river basins originating in the Tibetan Plateau and has major implications for hydrological processes (Bookhagen & Burbank, 2006; Bernard et al., 2010).

Superimposed on this gradient is a complex spatial pattern of precipitation. Rainfall is highest across the central portion of the basin due to the influence of the Southwest Monsoon, while both the upper and lower reaches exhibit greater variability and lower mean annual precipitation (Lauri et al., 2012; Mainuddin & Kirby, 2009; Mekong River Commission, 2010). Such spatial heterogeneity in rainfall is consistent with monsoon-driven hydrology observed throughout Southeast Asia (Huo & Peltier, 2021; Yatagai et al., 2012).

The juxtaposition of rapidly decreasing

elevation with a non-uniform rainfall pattern highlights the combined roles of topography and climate in shaping runoff generation across the MRB. Steep upstream terrain promotes rapid runoff production and limited soil-water retention, whereas flatter downstream landscapes enhance infiltration, storage, and delayed hydrological response (Beven & Kirkby, 1979; Western et al., 2002). These interactions help explain the observed differences among sub-basins in soil moisture dynamics, streamflow characteristics, and drought sensitivity, underscoring the importance of considering both climatic and geomorphological controls in assessing basin-wide droughts.

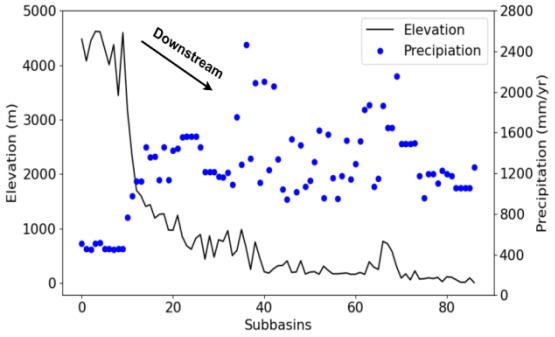


Figure 7. Longitudinal variation of elevation and precipitation across subbasins of the MRB

The following is Fig. 8, which shows the elevations and slopes of six subbasins as a function of their annual precipitation. The UMRB has the highest elevation, exceeding 4,500 m, and the lowest annual precipitation, and is characterized by high-altitude continental and temperate climates that are less influenced by monsoon circulation. As shown in Fig. 8b, the annual precipitation of both 3S and MMB-2 is much higher than that of Chi-Mun and LMRB. Considering the Indian monsoon extent fully covers these four subbasins, the windward sides (i.e., 3S and MMB-2) of the Indian monsoon will have higher precipitation than the leeward sides (i.e., Chi-Mun and LMRB) as compared with Fig. 1 by Delgado et al. (2012). Although the windward sides (i.e., Chi-Mun and LMRB) of the East Asia-Western North Pacific monsoon are expected to have higher precipitation than the leeward sides (i.e., 3S and MMB-2), only part of the Chi-Mun and LMRB subbasins is influenced by the East Asia-Western North Pacific monsoon, which might hinder such orographic effects. Both the elevations and slopes of 3S and MMB-2 are higher and steeper than those of Chi-Mun and LMRB, which will further exaggerate orographic effects fully covered by the Indian monsoon.

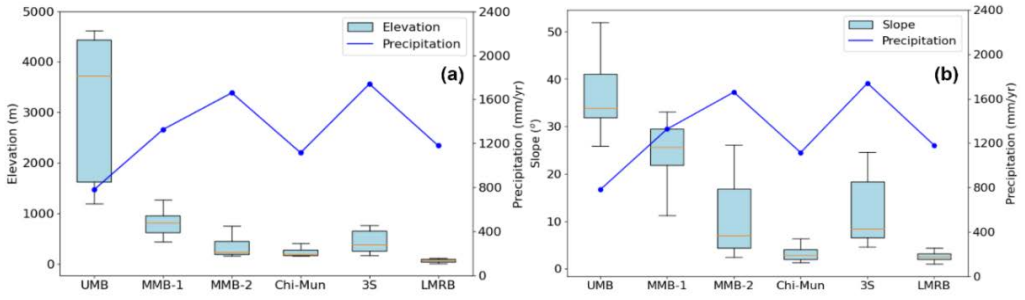


Figure 8. (a) Elevation and annual precipitation, and (b) slope and annual precipitation of the MRB subbasins

3.4. Historical features of the droughts

Drought events in the MRB have become increasingly frequent and intense in recent decades, posing significant challenges to regional water resources and agricultural systems. Figure 9 presents the temporal evolution of three drought indices (SPI,

SSWI, and SRI) at accumulation scales of 3, 6, and 12 months during 1970–2000. The three indices exhibit consistent temporal variability, with simultaneous declines during major drought periods, indicating strong coupling between meteorological forcing, soil moisture depletion, and streamflow reduction.

Figure 9 shows consistent temporal variability among SPI, SSWI, and SRI across the study period, with major drought episodes characterized by simultaneous decreases in all three indices. Distinct drought events are identified around 1972, 1983, 1990, 1992, 1995, and 1998, during which the indices frequently fell below -1 and occasionally reached -2 or lower, indicating severe drought conditions. The concurrence of negative anomalies among precipitation, soil moisture, and streamflow indices suggests that major drought episodes affected multiple components of the hydrological system. However, differences in magnitude and persistence are evident among the three indices.

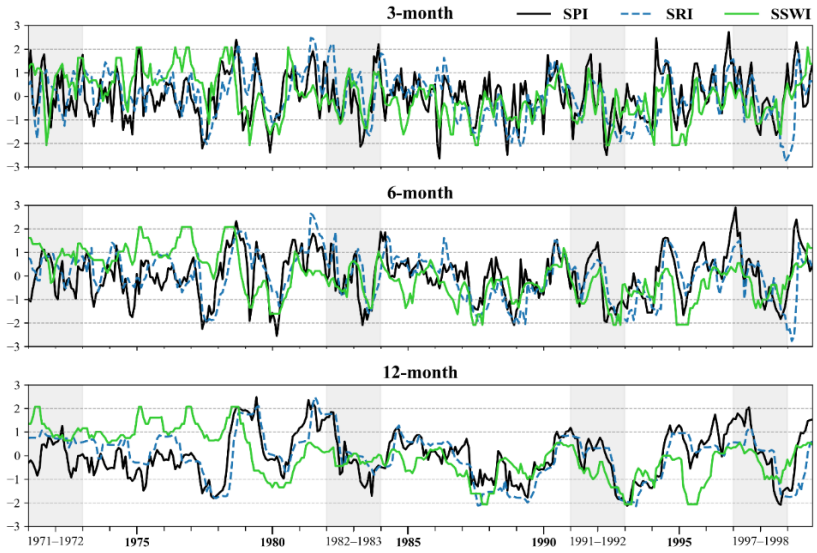


Figure 9. SPI, SRI, and SSWI at 3-, 6-, and 12-month accumulation scales

Among these events, the 1991–1992 drought is particularly pronounced. At the 3-month scale, SPI reaches approximately -2.50, while SSWI and SRI decrease to about -2.08 and -1.92, respectively, indicating an extreme meteorological drought followed by substantial soil moisture depletion and streamflow reduction. Compared to the 1982–1983 and 1997–1998 events, the 1991–1992 drought shows a more sustained decline across all indices, especially at longer accumulation scales, suggesting stronger persistence and a more pronounced hydrological response. The event persists over multiple consecutive months, highlighting its duration and severity. The concurrent reductions in SPI, SSWI, and SRI suggest strong interactions among meteorological, agricultural, and hydrological drought conditions during severe drought events.

The influence of the accumulation scale further clarifies drought persistence and propagation. While the 3-month indices capture rapid fluctuations associated with short-term precipitation deficits, the 6- and 12-month indices capture smoother, longer-lasting drought conditions, suggesting that hydrological drought is more persistent than meteorological drought.

Several drought events coincide with El Niño episodes, particularly during 1971–1972, 1982–1983, 1991–1992, and 1997–1998, highlighting the influence of the El Niño-Southern Oscillation (ENSO) on hydroclimatic variability in the MRB (CCAFS-SEA, 2016; Ropelewski & Halpert, 1987). Among these, the 1991–1992 event stands out as the most severe, characterized by the lowest index values and the strongest co-occurrence of meteorological, agricultural, and hydrological drought signals. Nevertheless, variations in drought severity and duration suggest that, beyond ENSO forcing, regional hydrological processes and antecedent moisture conditions also modulate drought development at the basin scale (Faranda et al., 2025; Vicente-Serrano et al., 2010).

To quantitatively assess the influence of ENSO on regional water scarcity, the frequency of severe drought conditions (Index < -1.5) during El Niño episodes was compared with the long-term baseline over the entire study period (Table 4).

Table 4. Severe drought occurrence during El Niño versus the full study period

Index	Entire period (%)	El Niño (%)	Ratio (El Niño/ All)
SPI	7.8	18.2	2.3
SRI	9.6	24.5	2.6
SSWI	10.1	29.8	2.9

The results clearly show a substantial increase in drought frequency during El Niño conditions. Specifically, the proportion of severe drought months increases from 7.8% to 18.2% for SPI, from 9.6% to 24.5% for SRI, and from 10.1% to 29.8% for SSWI. These correspond to approximately 2.3-, 2.6-, and 2.9-fold increases, respectively.

Notably, the magnitude of increase becomes more pronounced from meteorological to hydrological and groundwater systems, with SSWI exhibiting the strongest response. This suggests that groundwater storage amplifies drought signals more strongly than precipitation and surface water indicators.

This pattern indicates that severe drought conditions become more pronounced in soil moisture and runoff deficits under El Niño conditions.

The statistical relationships among the drought indices are summarized in Table 5. The correlation between SPI and SRI increases from 0.42 at the 3-month scale to 0.58 at the 6-month scale and 0.75 at the 12-month scale, suggesting that hydrological drought becomes more strongly associated with long-term precipitation deficits. This pattern likely reflects the delayed response of river discharge and the influence of basin-scale hydrological memory. In large monsoon-dominated basins such as the MRB, precipitation anomalies may be progressively integrated through soil moisture storage, groundwater contributions, and basin-scale water retention before influencing streamflow. As a result, hydrological drought tends to develop more gradually and shows stronger correspondence with precipitation deficits at longer accumulation periods.

In contrast, the correlation between SPI and SSWI decreases from 0.50 at the 3-month scale to 0.39 and 0.26 at the 6- and 12-month scales, respectively, suggesting that soil moisture responds more rapidly to short-term precipitation variability than streamflow. This behavior may be influenced by soil hydraulic properties and evapotranspiration processes, which control the rate at which rainfall anomalies affect soil water availability. In tropical monsoon environments such as the MRB, high evapotranspiration and seasonal rainfall variability can amplify short-term soil moisture fluctuations, while deeper hydrological storage components buffer streamflow response. These differences suggest that precipitation, soil moisture, and streamflow exhibit different temporal responses and persistence characteristics.

Table 5. Pearson correlation coefficients between drought indices for different accumulation periods in the Mekong River basin

	SPI3	**SPI6**	**SPI12**	**SRI3**	**SRI6**	**SRI12**	**SSWI3**	**SSWI6**	**SSWI12**
SPI3	1.00								
SPI6	0.61	1.00							
SPI12	0.35	0.59	1.00						
SRI3	0.42	0.64	0.65	1.00					
SRI6	0.26	0.58	**0.74**	**0.85**	1.00				
SRI12	0.10	0.31	**0.75**	0.62	**0.76**	1.00			
SSWI3	0.50	0.35	0.06	0.32	0.21	0.04	1.00		
SSWI6	0.35	0.39	0.12	0.40	0.34	0.14	**0.78**	1.00	
SSWI12	0.21	0.27	0.26	0.40	0.42	0.34	0.60	**0.81**	1.00

Overall, these results highlight the potential roles of basin storage capacity, groundwater buffering, soil hydraulic characteristics, and evapotranspiration dynamics in shaping the temporal and spatial characteristics of meteorological, agricultural, and hydrological droughts. However, these interpretations are based on inferred mechanisms and would benefit from further process-based analyses in future studies.

3.5. Spatial variability of soil moisture and implications for agricultural drought characteristics

Soil moisture is a key state variable linking atmospheric forcing to land surface hydrological processes and therefore provides valuable information for characterizing agricultural drought conditions. Previous studies have shown that soil moisture variability generally increases during dry periods because of heterogeneities in vegetation cover, soil properties, and topography, whereas widespread rainfall tends to homogenize soil moisture conditions during wet periods (Ivanov et al., 2010; Srivastava et al., 2021). Consequently, investigating the spatial variability of soil moisture can provide additional insights into regional differences in hydrological responses and agricultural drought characteristics.

The Mekong River Basin exhibits pronounced geomorphological and pedological contrasts between the UMRB and the LMRB, which are associated with different soil moisture storage characteristics. Steep mountainous terrain in the upstream region generally favors rapid runoff generation and limited water retention. In contrast, extensive floodplains and groundwater interactions in the downstream region enhance basin storage and promote more persistent soil moisture conditions. These contrasting characteristics may contribute to spatial heterogeneity in soil moisture and agricultural drought characteristics across the basin.

To investigate these regional differences, the spatial coefficient of variation (CV) of soil moisture was calculated for the UMRB and the LMRB during the severe drought year of 1992 (Fig. 10). The results reveal clear contrasts between upstream and downstream regions, with the UMRB exhibiting substantially higher CV values, indicating more heterogeneous soil moisture conditions. Consistent with previous studies, spatial variability tends to increase during dry periods and decrease under wetter conditions (Poltoradnev et al., 2016; Rosenbaum et al., 2012). Moreover, distinct seasonal responses are observed between the two sub-basins, suggesting different patterns of soil moisture dynamics during drought conditions.

In the UMRB (Fig. 10a, c), soil moisture exhibits pronounced fluctuations throughout the year, and spatial variability remains relatively high even during wetting periods.

This pattern reflects strong topographic control and uneven precipitation distribution in the mountainous upstream region. Local infiltration processes, lateral redistribution of soil water, and limited basin storage capacity contribute to strong spatial contrasts in soil moisture conditions. These conditions promote rapid and spatially uneven development of agricultural drought signals in the upstream region.

In contrast, the LMRB (Fig. 10b, d) shows a clear reduction in spatial variability during the wet season as precipitation increases. Widespread monsoon rainfall across the relatively flat downstream floodplain homogenizes soil moisture conditions. In addition, extensive floodplain storage and groundwater interactions enhance hydrological buffering, allowing precipitation anomalies to be integrated over broader spatial scales. As a result, agricultural drought signals tend to propagate more gradually and coherently downstream into the floodplain.

These contrasting responses highlight the important roles of topography, storage capacity, and hydrological buffering in controlling soil moisture heterogeneity and shaping agricultural drought characteristics across the MRB. The observed differences between the upstream and downstream regions suggest that basin physiographic properties strongly influence the spatial distribution and persistence of drought conditions, thereby improving our understanding of the processes governing drought development within the basin.

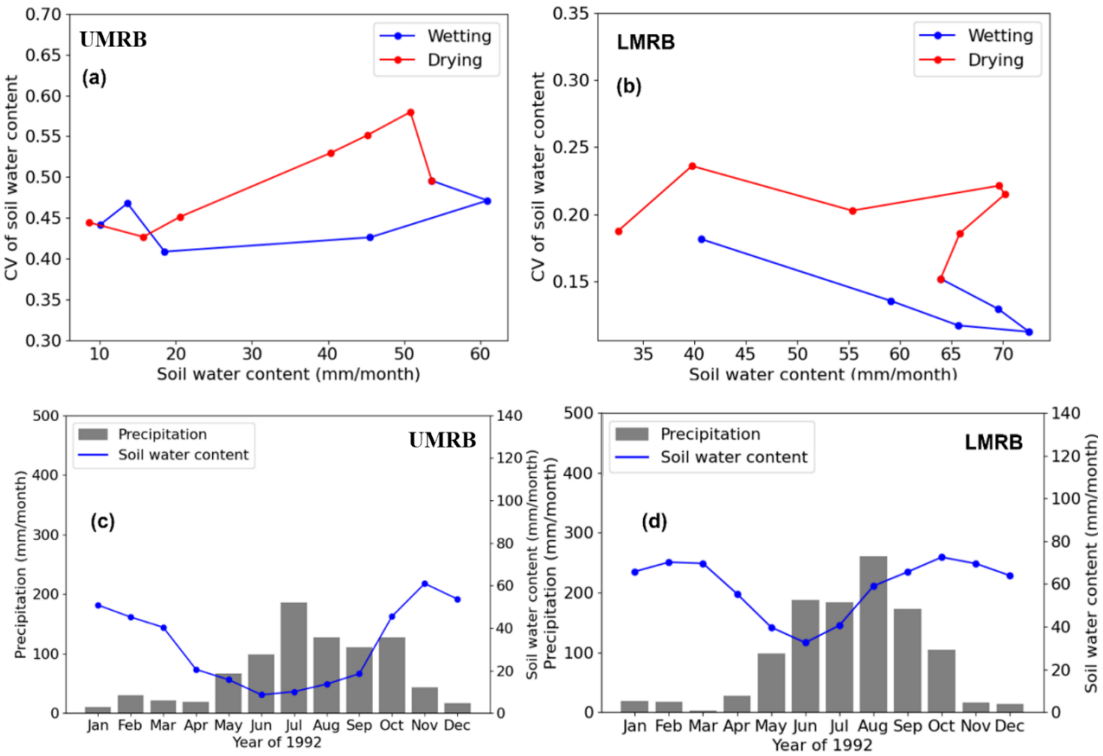


Figure 10. Relationship between the coefficient of variation of soil water content and mean soil water content in (a) the UMRB and (b) the LMRB in 1992. Monthly precipitation and soil water content in (c) the UMRB and (d) the LMRB in 1992. Figures a-b adapted from Nguyen et al. (2023), with permission from Elsevier, License No. 502056156

4. Conclusions

This study employed the SWAT model to simulate streamflow and examine the dynamics of meteorological, agricultural, and hydrological droughts across the MRB using the SPI, SSWI, and SRI indices. The model achieved satisfactory to very good performance at daily and monthly scales, suggesting its ability to reproduce the basin's general seasonal hydrological behavior. However, increased uncertainties at downstream stations likely reflect the influence of reservoir operations, land-use changes, and complex hydro-geomorphological conditions, which should be considered when interpreting model-based drought indicators.

Furthermore, the integrated analysis suggests generally consistent drought signals among SPI, SSWI, and SRI, indicating strong consistency among meteorological, agricultural, and hydrological drought signals. Stronger correlations among indices at longer accumulation periods may reflect increased coupling during extended dry conditions; however, these relationships are primarily assessed at the basin scale and may not fully represent spatial heterogeneity.

Model simulations also indicate potential spatial differences in soil moisture persistence among sub-basins, which topography, soil properties, and evapotranspiration may influence. However, these patterns are subject to model limitations and should be interpreted with caution. Further validation using in situ observations or satellite-based datasets will be necessary in future studies to better constrain these spatial dynamics.

Meanwhile, the influence of large-scale climate variability, particularly the ENSO, is qualitatively suggested by the coincidence of major drought events with El Niño periods. However, this relationship has not been quantitatively evaluated in this study and requires further analysis using dedicated climate indices (e.g., ONI).

Overall, this study highlights the potential of combining hydrological modeling with multiple drought indicators to explore drought dynamics in large transboundary basins. While the findings provide preliminary process-based insights, further work incorporating observational data, spatial analyses, and quantitative climate assessments is needed to better constrain the mechanisms and drivers of drought across the MRB.

Acknowledgments

We would like to thank the Vietnam National Foundation for Science and Technology Development (NAFOSTED) for funding the research project "Surface and groundwater interaction in the Mekong River Basin: Novel Ensemble Machine Learning Approaches" under Grant Number 105.06-2023.02.

References

Abbaspour K.C., 2013. SWAT-CUP 2012: SWAT calibration and uncertainty programs-a user manual. Eawag: Dübendorf, Switzerland, 103. https://www.mdpi.com/2073-4441/9/6/384.

Abbaspour K.C., Vejdani M., Haghighat S., Yang J., 2007. SWAT-CUP calibration and uncertainty programs for SWAT. In MODSIM 2007 international congress on modelling and simulation, modelling and simulation society of Australia and New Zealand. Dübendorf, Switzerland: Swiss Federal Institute of Aquatic Science and Technology, 1596–1602.

Abou Rafee S.A., Uvo C.B., Martins J.A., Domingues L.M., Rudke A.P., Fujita T., Freitas E.D., 2019. Large-scale hydrological modelling of the Upper Paraná River Basin. Water, 11(5), 882. https://doi.org/10.3390/w11050882.

Arnold J.G., Srinivasan R., Muttiah R.S., Williams J.R., 1998. Large area hydrologic modeling and assessment part I: model development 1. JAWRA Journal of the American Water Resources Association, 34(1), 73–89. https://doi.org/10.1111/j.1752-1688.1998.tb05961.x.

Bernard, A., Lécuyer C., Vincent P., Amiot R., Bardet N., Buffetaut E., Cuny G., Fourel F., Martineau F.,

Prieur, A., 2010. Regulation of body temperature by some Mesozoic marine reptiles. Science, 328(5984), 1379–1382. https://doi.org/10.1126/science.1187443.

Beven K.J., Kirkby M.J., 1979. A physically based, variable contributing area model of basin hydrology/Un modèle à base physique de zone d'appel variable de l'hydrologie du bassin versant. Hydrological Sciences Journal, 24(1), 43–69. https://doi.org/10.1080/02626667909491834.

Binh D. Van, Kantoush S., Sumi T., 2020. Changes to long-term discharge and sediment loads in the Vietnamese Mekong Delta caused by upstream dams. Geomorphology, 353, 107011. https://doi.org/10.1016/j.geomorph.2019.107011.

Bookhagen B., Burbank D.W., 2006. Topography, relief, and TRMM-derived rainfall variations along the Himalaya. Geophysical research letters, 33(8). https://doi.org/10.1029/2006GL026037.

CCAFS-SEA (CGIAR Research Program on Climate Change A. and F.S.-S. A.), 2016. The drought crisis in the Central Highlands of Vietnam Assessment Report CGIAR Research Centers in Southeast Asia, 1–35.

Cosslett T.L., Cosslett P.D., 2017. Sustainable development of rice and water resources in Mainland Southeast Asia and Mekong River Basin. Springer. https://doi.org/10.1007/978-981-10-5613-0.

Dai A., 2011. Characteristics and trends in various forms of the Palmer Drought Severity Index during 1900–2008. Journal of Geophysical Research: Atmospheres, 116(D12). https://doi.org/10.1029/2010JD015541.

Dang T.D., Chowdhury A.K., Galelli S., 2020. On the representation of water reservoir storage and operations in large-scale hydrological models: implications on model parameterization and climate change impact assessments. Hydrology and Earth System Sciences, 24(1), 397–416. https://doi.org/10.5194/hess-24-397-2020.

Delgado J.M., Merz B., Apel H., 2012. A climate-flood link for the lower Mekong River. Hydrology and Earth System Sciences, 16(5), 1533–1541. https://doi.org/10.5194/hess-16-1533-2012.

Dong Z., Liu H., Hu H., Khan M.Y.A., Wen J., Chen L., Tian F., 2022. Future projection of seasonal drought characteristics using CMIP6 in the Lancang-Mekong River Basin. Journal of Hydrology, 610, 127815. https://doi.org/10.1016/j.jhydrol.2022.127815.

Duan K., Mei Y., 2014. Comparison of meteorological, hydrological and agricultural drought responses to climate change and uncertainty assessment. Water resources management, 28(14), 5039–5054. https://doi.org/10.1007/s11269-014-0789-6.

Faranda D., Sato Y., Dong C., Gualandi A., Noyelle R., Alberti T., Dubrulle B., Fery L., Messori G., Vrac M., El Niño al, Vaittinada Ayar P., Yiou P., Mengaldo G., 2025. El Niño and droughts in Southeast Asia: A stochastic-chaotic modeling approach. Physical Review E, 111(6–1), 064209. https://doi.org/10.1103/PhysRevE.111.064209ï.

Fuka D.R., Walter M.T., Macalister C., Degaetano A.T., Steenhuis T.S., Easton Z.M., 2014. Using the Climate Forecast System Reanalysis as weather input data for watershed models. Hydrological Processes, 28(22), 5613–5623. https://doi.org/10.1002/hyp.10073.

Gassman P.W., Sadeghi A.M., Srinivasan R., 2014. Applications of the SWAT Model Special Section: overview and insights. Journal of Environmental Quality, 43(1), 1–8. https://doi.org/10.2134/jeq2013.11.0466.

Ghaith M., Li Z., 2020. Propagation of parameter uncertainty in SWAT: A probabilistic forecasting method based on polynomial chaos expansion and machine learning. Journal of Hydrology, 586, 124854. https://doi.org/10.1016/j.jhydrol.2020.124854.

Grayson R.B., Moore I.D., McMahon T.A., 1992. Physically based hydrologic modeling: 2. Is the concept realistic?. Water resources research, 28(10), 2659–2666. https://doi.org/10.1029/92WR01259.

Gunten D. Von, Wöhling T., Haslauer C.P., Merchán D., Causapé J., Cirpka O.A., 2016. Using an integrated hydrological model to estimate the usefulness of meteorological drought indices in a changing climate. Hydrology and Earth System Sciences, 20(10), 4159–4175. https://doi.org/10.5194/hess-20-4159-2016.

Guo H., Bao A., Liu T., Ndayisaba F., He D., Kurban A., De Maeyer P., 2017. Meteorological drought analysis in the Lower Mekong Basin

using satellite-based long-term CHIRPS product. Sustainability (Switzerland), 9(6), 901. https://doi.org/10.3390/su9060901.

Guo Y., Huang S., Huang Q., Leng G., Fang W., Wang L., Wang H., 2020. Propagation thresholds of meteorological drought for triggering hydrological drought at various levels. Science of the Total Environment, 712, 136502. https://doi.org/10.1016/j.scitotenv.2020.136502.

He F., Thieme M., Zarfl C., Grill G., Lehner B., Hogan Z., Tockner K., Jähnig S.C., 2021. Impacts of loss of free-flowing rivers on global freshwater megafauna. Biological Conservation, 263, 109335. https://doi.org/10.1016/j.biocon.2021.109335.

He X., Wada Y., Wanders N., Sheffield J., 2017. Intensification of hydrological drought in California by human water management. Geophysical Research Letters, 44(4), 1777–1785. https://doi.org/10.1002/2016GL071665.

Huo Y., Peltier W.R., 2021. The southeast asian monsoon: dynamically downscaled climate change projections and high resolution regional ocean modelling on the effects of the Tibetan Plateau. Climate Dynamics, 56(7), 2597–2616. https://doi.org/10.1007/s00382-020-05604-9.

Inseeyong N., Hu H., Chuenchum P., Yu B., Xu M., 2024. Staged SWAT calibration with bias-corrected precipitation product for enhancing flow data continuity in tributaries of the Mekong River. Science of the Total Environment, 934, 173291. https://doi.org/10.1016/j.scitotenv.2024.173291.

Ivanov V.Y., Fatichi S., Jenerette G.D., Espeleta J.F., Troch P.A., Huxman T.E., 2010. Hysteresis of soil moisture spatial heterogeneity and the "homogenizing" effect of vegetation. Water Resources Research, 46(9). https://doi.org/10.1029/2009WR008611.

Kamali B., Houshmand Kouchi D., Yang H., Abbaspour K.C., 2017. Multilevel drought hazard assessment under climate change scenarios in semi-arid regions-a case study of the Karkheh river basin in Iran. Water, 9(4), 241. https://doi.org/10.3390/w9040241.

Kang H., Sridhar V., 2021. A near-term drought assessment using hydrological and climate forecasting in the Mekong River Basin. International Journal of Climatology, 41, E2497-E2516. https://doi.org/10.1002/joc.6860.

Kang H., Sridhar V., Mainuddin M., Trung L.D., 2021. Future rice farming threatened by drought in the Lower Mekong Basin. Scientific reports, 11(1), 9383. https://doi.org/10.1038/s41598-021-88405-2.

Keovilignavong O., Nguyen T. H., Hirsch P., 2023. Reviewing the causes of Mekong drought before and during 2019–20. International Journal of Water Resources Development, 39(1), 155–175. https://doi.org/10.1080/07900627.2021.1967112.

Knoben W.J., Freer J.E., Woods R.A., 2019. Inherent benchmark or not? Comparing Nash-Sutcliffe and Kling–Gupta efficiency scores. Hydrology and Earth System Sciences, 23(10), 4323–4331. https://doi.org/10.5194/hess-23-4323-2019.

Konapala G., Mishra A.K., Wada Y., Mann M.E., 2020. Climate change will affect global water availability through compounding changes in seasonal precipitation and evaporation. Nature communications, 11(1), 3044. https://doi.org/10.1038/s41467-020-16757-w.

Kondolf G.M., Rubin Z.K., Minear J.T., 2014. Dams on the Mekong: Cumulative sediment starvation. Water Resources Research, 50(6), 5158–5169. https://doi.org/10.1002/2013WR014651.

Lauri H., de Moel H., Ward P.J., Räsänen T.A., Keskinen M., Kummu M., 2012. Future changes in Mekong River hydrology: impact of climate change and reservoir operation on discharge. Hydrology and Earth system sciences, 16(12), 4603–4619. https://doi.org/10.5194/hess-16-4603-2012.

Lauri H., Räsänen T.A., Kummu M., 2014. Using reanalysis and remotely sensed temperature and precipitation data for hydrological modeling in monsoon climate: Mekong River case study. Journal of Hydrometeorology, 15(4), 1532–1545. https://doi.org/10.1175/JHM-D-13-084.1.

Le X.H., Kim Y., Van Binh D., Jung S., Nguyen D.H., Lee G., 2024. Improving rainfall-runoff modeling in the Mekong river basin using bias-corrected satellite precipitation products by convolutional neural networks. Journal of Hydrology, 630, 130762. https://doi.org/10.1016/j.jhydrol.2024.130762.

Lee S.K., Dang T.A., 2019. Spatio-temporal variations in meteorology drought over the Mekong River Delta of Vietnam in the recent decades. Paddy and Water Environment, 17(1), 35–44. https://doi.org/10.1007/s10333-018-0681-8.

Leng G., Tang Q., Rayburg S., 2015. Climate change impacts on meteorological, agricultural and

hydrological droughts in China. Global and Planetary Change, 126, 23–34. https://doi.org/10.1016/j.gloplacha.2015.01.003.

Li C., Fang H., 2021. Assessment of climate change impacts on the streamflow for the Mun River in the Mekong Basin, Southeast Asia: Using SWAT model. Catena, 201, 105199. https://doi.org/10.1016/j.catena.2021.105199.

Li M., Di Z., Duan Q., 2021. Effect of sensitivity analysis on parameter optimization: Case study based on streamflow simulations using the SWAT model in China. Journal of Hydrology, 603, 126896. https://doi.org/10.1016/j.jhydrol.2021.126896.

Li Y., Lu H., Yang K., Wang W., Tang Q., Khem S., Yang F., Huang Y., 2021. Meteorological and hydrological droughts in Mekong River Basin and surrounding areas under climate change. Journal of Hydrology: Regional Studies, 36, 100873. https://doi.org/10.1016/j.ejrh.2021.100873.

Loc H.H., Van Binh D., Park E., Shrestha S., Dung T.D., Son V.H., Truc N.H.T., Mai N.P., Seijger C., 2021. Intensifying saline water intrusion and drought in the Mekong Delta: From physical evidence to policy outlooks. Science of the Total Environment, 757, 143919. https://doi.org/10.1016/j.scitotenv.2020.143919.

Lu X.X., Li S., Kummu M., Padawangi R., Wang J.J., 2014. Observed changes in the water flow at Chiang Saen in the lower Mekong: Impacts of Chinese dams?. Quaternary International, 336, 145–157. https://doi.org/10.1016/j.quaint.2014.02.006.

Mainuddin M., Kirby M., 2009. Spatial and temporal trends of water productivity in the lower Mekong River Basin. Agricultural Water Management, 96(11), 1567–1578. https://doi.org/10.1016/j.agwat.2009.06.013.

McCuen R.H., Knight Z., Cutter A.G., 2006. Evaluation of the Nash-Sutcliffe efficiency index. Journal of hydrologic engineering, 11(6), 597–602. https://doi.org/10.1061/(ASCE)1084-0699(2006)11:6(597).

Mekong River Commission, 2005. Overview of the Hydrology of the Mekong Basin Mekong River Commission. Meeting the Needs, Keeping the Balance, 73p.

Mekong River Commission, 2010. Social Impact Monitoring and Vulnerability Assessment: Report on a Regional Pilot Study for the Mekong Corridor (No. 30). Mekong River Commission.

Mishra A.K., Singh V.P., 2010. A review of drought concepts. Journal of hydrology, 391(1-2), 202–216. https://doi.org/10.1016/j.jhydrol.2010.07.012.

Mohammed I.N., Bolten J.D., Srinivasan R., Lakshmi V., 2018. Satellite observations and modeling to understand the Lower Mekong River Basin streamflow variability. Journal of hydrology, 564, 559–573. https://doi.org/10.1016/j.jhydrol.2018.07.030.

Moriasi D.N., Arnold J.G., Van Liew M.W., Bingner R.L., Harmel R.D., Veith T.L., 2007. Model evaluation guidelines for systematic quantification of accuracy in watershed simulations. Transactions of the ASABE, 50(3), 885–900. https://doi.org/10.13031/2013.23153.

Moriasi D.N., Wilson B.N., Douglas-Mankin K.R., Arnold J.G., Gowda P.H., 2012. Hydrologic and water quality models: Use, calibration, and validation. Transactions of the ASABE, 55(4), 1241–1247. https://doi.org/10.13031/2013.42265.

Mukundan R., Radcliffe D.E., Risse L.M., 2010. Spatial resolution of soil data and channel erosion effects on SWAT model predictions of flow and sediment. Journal of soil and water conservation, 65(2), 92–104. https://doi.org/10.2489/jswc.65.2.92.

Nguyen H., Shaw R., 2011. Adaptation to droughts in Cambodia. https://doi.org/10.1108/S2040-7262(2011)0000008009.

Nguyen T.T.H., Li M.H., Vu T.M., Chen P.Y., 2023. Multiple drought indices and their teleconnections with ENSO in various spatiotemporal scales over the Mekong River Basin. Science of the Total Environment, 854, 158589.. https://doi.org/10.1016/j.scitotenv.2022.158589

Ogston A.S., Allison M.A., McLachlan R.L., Nowacki D.J., Stephens J.D., 2017. How tidal processes impact the transfer of sediment from source to sink: Mekong river collaborative studies. Oceanography, 30(3), 22–33. https://www.jstor.org/stable/26201895.

Pandey S., Bhandari H.S., Hardy B., 2007. Economic costs of drought and rice farmers' coping mechanisms: a cross-country comparative analysis. Int. Rice Res. Inst.

Phi Hoang L., Lauri H., Kummu M., Koponen J., Vliet M.T.H.V., Supit I., Leemans R., Kabat P., Ludwig, F. (2016). Mekong River flow and hydrological extremes under climate change. Hydrology and

Earth System Sciences, 20(7), 3027–3041. https://doi.org/10.5194/hess-20-3027-2016.

Poltoradnev M., Ingwersen J., Streck T., 2016. Spatial and temporal variability of soil water content in two regions of southwest Germany during a three-year observation period. Vadose Zone Journal, 15(6), vzj2015-11. https://doi.org/10.2136/vzj2015.11.0143.

Qiu J., 2010. China drought highlights future climate threats. Nature, 465, 142–143. https://doi.org/10.1038/465142a.

Räsänen T.A., Kummu M., 2013. Spatiotemporal influences of ENSO on precipitation and flood pulse in the Mekong River Basin. Journal of Hydrology, 476, 154–168. https://doi.org/10.1016/j.jhydrol.2012.10.028.

Räsänen T.A., Lindgren V., Guillaume J.H., Buckley B.M., Kummu M., 2016. On the spatial and temporal variability of ENSO precipitation and drought teleconnection in mainland Southeast Asia. Climate of the Past, 12(9), 1889–1905. https://doi.org/10.5194/cp-12-1889-2016.

Räsänen T.A., Someth P., Lauri H., Koponen J., Sarkkula J., Kummu M., 2017. Observed river discharge changes due to hydropower operations in the Upper Mekong Basin. Journal of Hydrology, 545, 28–41. https://doi.org/10.1016/j.jhydrol.2016.12.023.

Rasmusson E.M., Carpenter T.H., 1982. Variations in Tropical Sea Surface Temperature and Surface Wind Fields Associated with the Southern Oscillation/El Niño. Monthly weather review, 110(5), 354–384. https://doi.org/10.1175/1520-0493(1982)110%3C0354:VITSST%3E2.0.CO;2.

Ropelewski C.F., Halpert M.S., 1987. Global and Regional Scale Precipitation Patterns Associated with the El Nino/Southern Oscillation. Monthly weather review, 115(8). 1606–1626. https://doi.org/10.1175/1520-0493(1987)115%3C1606:GARSPP%3E2.0.CO;2.

Rosenbaum U., Bogena H.R., Herbst M., Huisman J.A., Peterson T.J., Weuthen A., Western A.W., Vereecken H., 2012. Seasonal and event dynamics of spatial soil moisture patterns at the small catchment scale. Water resources research, 48(10). https://doi.org/10.1029/2011WR011518.

Sam T.T., Khoi D.N., Thao N.T.T., Nhi P.T.T., Quan N.T., Hoan N.X., Nguyen V.T., 2019. Impact of climate change on meteorological, hydrological and agricultural droughts in the Lower Mekong River Basin: a case study of the Srepok Basin, Vietnam. Water and Environment Journal, 33(4), 547–559. https://doi.org/10.1111/wej.12424.

Saxton K.E., Rawls W.J., 2006. Soil Water Characteristic Estimates by Texture and Organic Matter for Hydrologic Solutions. Soil Science Society of America Journal, 70(5), 1569–1578. https://doi.org/10.2136/sssaj2005.0117.

Seneviratne S.I., Corti T., Davin E.L., Hirschi M., Jaeger E.B., Lehner I., Orlowsky B., Teuling A.J., 2010. Investigating soil moisture–climate interactions in a changing climate: A review. Earth-Science Reviews, 99(3–4), 125–161. https://doi.org/10.1016/j.earscirev.2010.02.004.

Sheffield J., Ziegler A.D., Wood E.F., Chen Y., 2004. Correction of the high-latitude rain day anomaly in the NCEP–NCAR reanalysis for land surface hydrological modeling. Journal of Climate, 17(19), 3814–3828. https://doi.org/10.1175/1520-0442(2004)017%3C3814:COTHRD%3E2.0.CO;2.

Shukla S., Wood A.W., 2008. Use of a standardized runoff index for characterizing hydrologic drought. Geophysical research letters, 35(2). https://doi.org/10.1029/2007GL032487.

Son N.T., Chen C.F., Chen C.R., Chang L.Y., Minh V.Q., 2012. Monitoring agricultural drought in the Lower Mekong Basin using MODIS NDVI and land surface temperature data. International Journal of Applied Earth Observation and Geoinformation, 18, 417–427. https://doi.org/10.1016/j.jag.2012.03.014.

Soukhaphon A., Baird I.G., Hogan Z.S., 2021. The impacts of hydropower dams in the Mekong River Basin: A review. Water, 13(3), 265. https://doi.org/10.3390/w13030265.

Srivastava, A., Saco P.M., Rodriguez J.F., Kumari N., Chun K.P., Yetemen O., 2020. The role of landscape morphology on soil moisture variability in semi-arid ecosystems. Hydrological Processes. Doi: 10.1002/hyp.13990.

Tang Q., 2020. Global change hydrology: Terrestrial water cycle and global change. Science China. Earth Sciences, 63(3), 459–462. https://doi.org/10.1007/s11430-019-9559-9.

Tang X., Zhang J., Gao C., Ruben G.B., Wang G., 2019. Assessing the uncertainties of four precipitation products for SWAT modeling in Mekong River Basin. Remote Sensing, 11(3), 304. https://doi.org/10.3390/rs11030304.

Thilakarathne M., Sridhar V., 2017. Characterization of future drought conditions in the Lower Mekong River Basin. Weather and Climate Extremes, 17, 47–58. https://doi.org/10.1016/j.wace.2017.07.004.

Tran T.N.D., Nguyen B.Q., Zhang R., Aryal A., Grodzka-Łukaszewska M., Sinicyn G., Lakshmi V., 2023. Quantification of gridded precipitation products for the streamflow simulation on the Mekong River basin using rainfall assessment framework: A case study for the Srepok River subbasin, Central Highland Vietnam. Remote Sensing, 15(4), 1030. https://doi.org/10.3390/rs15041030.

Trang N.T.T., Shrestha S., Shrestha M., Datta A., Kawasaki A., 2017. Evaluating the impacts of climate and land-use change on the hydrology and nutrient yield in a transboundary river basin: A case study in the 3S River Basin (Sekong, Sesan, and Srepok). Science of the Total Environment, 576, 586–598. https://doi.org/10.1016/j.scitotenv.2016.10.138.

Tuo Y., Duan Z., Disse M., Chiogna G., 2016. Evaluation of precipitation input for SWAT modeling in Alpine catchment: A case study in the Adige river basin (Italy). Science of the total environment, 573, 66–82. https://doi.org/10.1016/j.scitotenv.2016.08.034.

Van Loon A.F., 2015. Hydrological drought explained. Wiley Interdisciplinary Reviews: Water, 2(4), 359–392. https://doi.org/10.1002/wat2.1085.

Van Loon A.F., Gleeson T., Clark J., Van Dijk A.I.J.M., Stahl K., Hannaford J., Di Baldassarre G., Teuling A.J., Tallaksen L.M., Uijlenhoet R., Hannah D.M., Sheffield J., Svoboda M., Verbeiren B., Wagener T., Rangecroft S., Wanders N., Van Lanen H.A.J., 2016. Drought in the Anthropocene. Nature Geoscience, 9(2), 89–91. https://doi.org/10.1038/ngeo2646.

Van Loon A.F., Van Lanen H.A., 2012. A process-based typology of hydrological drought. Hydrology and Earth System Sciences, 16(7), 1915–1946. https://doi.org/10.5194/hess-16-1915-2012.

Vicente-Serrano S.M., Beguería S., López-Moreno J.I., 2010. A multiscalar drought index sensitive to global warming: The standardized precipitation evapotranspiration index. Journal of Climate, 23(7), 1696–1718. https://doi.org/10.1175/2009JCLI2909.1.

Vu M.T., Raghavan S.V., Liong S.Y., 2012. SWAT use of gridded observations for simulating runoff-a Vietnam river basin study. Hydrology and Earth System Sciences, 16(8), 2801–2811. https://doi.org/10.5194/hess-16-2801-2012.

Vu M.T., Raghavan V.S., Liong S.Y., 2015a. Ensemble Climate Projection for Hydro-Meteorological Drought over a river basin in Central Highland, Vietnam. KSCE Journal of Civil Engineering, 19(2), 427–433. https://doi.org/10.1007/s12205-015-0506-x.

Vu M.T., Raghavan V.S., Liong S.Y., 2015b. Ensemble Climate Projection for Hydro-Meteorological Drought over a river basin in Central Highland, Vietnam. KSCE Journal of Civil Engineering, 19(2), 427–433. https://doi.org/10.1007/s12205-015-0506-x.

Vu M.T., Vo N.D., Gourbesville P., Raghavan S.V., Liong S.Y., 2017. Hydro-meteorological drought assessment under climate change impact over the Vu Gia-Thu Bon river basin, Vietnam. Hydrological Sciences Journal, 62(10), 1654–1668. https://doi.org/10.1080/02626667.2017.1346374.

Vu T.M., Mishra A.K., 2016. Spatial and temporal variability of standardized precipitation index over Indochina peninsula. Cuadernos de investigación geográfica: Geographical Research Letters, 42(1), 221–232. https://doi.org/10.18172/cig.2928.

Vu T.M., Raghavan S.V., Liong S.Y., Mishra A.K., 2018. Uncertainties of gridded precipitation observations in characterizing spatio-temporal drought and wetness over Vietnam. International Journal of Climatology, 38(4), 2067–2081. https://doi.org/10.1002/joc.5317.

Wang D., Hejazi M., Cai X., Valocchi A.J., 2011. Climate change impact on meteorological, agricultural, and hydrological drought in central Illinois. Water Resources Research, 47(9). https://doi.org/10.1029/2010WR009845.

Wang W., Lu H., Yang D., Sothea K., Jiao Y., Gao B., Peng X., Pang, Z., 2016. Modelling hydrologic processes in the Mekong River Basin using a distributed model driven by satellite precipitation and rain gauge observations. PloS one, 11(3), e0152229. https://doi.org/10.1371/journal.pone.0152229.

Wang Y., Bian J., Zhao Y., Tang J., Jia Z., 2018. Assessment of future climate change impacts on nonpoint source pollution in snowmelt period for a cold area using SWAT. Scientific reports, 8(1), 2402. https://doi.org/10.1038/s41598-018-20818-y.

Western A.W., Grayson R.B., Blöschl G., 2002. Scaling of soil moisture: A hydrologic perspective. Annual review of earth and planetary sciences, 30(1), 149–180. https://doi.org/10.1146/annurev.earth.30.091201.140434.

Wilhite D.A., 2000. Chapter 1 Drought as a Natural Hazard: Concepts and Definitions, 1(1), 3–18. http://digitalcommons.unl.edu/droughtfacpubhttp://digitalcommons.unl.edu/droughtfacpub/69.

Wu J., Chen X., Yu Z., Yao H., Li W., Zhang D., 2019. Assessing the impact of human regulations on hydrological drought development and recovery based on a 'simulated-observed'comparison of the SWAT model. Journal of Hydrology, 577, 123990. https://doi.org/10.1016/j.jhydrol.2019.123990.

Xue Z., Liu J.P., Ge Q., 2011. Changes in hydrology and sediment delivery of the Mekong River in the last 50 years: connection to damming, monsoon, and ENSO. Earth Surface Processes and Landforms, 36(3), 296–308. https://doi.org/10.1002/esp.2036.

Yatagai A., Kamiguchi K., Arakawa O., Hamada A., Yasutomi N., Kitoh A., 2012. Aphrodite: Constructing a long-term daily gridded precipitation dataset for Asia based on a dense network of rain gauges. Bulletin of the American Meteorological Society, 93(9), 1401–1415. https://doi.org/10.1175/BAMS-D-11-00122.1.

Yoshida Y., Lee H.S., Trung B.H., Tran H.D., Lall M.K., Kakar K., Xuan T.D., 2020. Impacts of mainstream hydropower dams on fisheries and agriculture in lower Mekong Basin. Sustainability, 12(6), 2408. https://doi.org/10.3390/su12062408.

Zhang X., Hao Z., Singh V.P., Zhang Y., Feng S., Xu Y., Hao F., 2022. Drought propagation under global warming: Characteristics, approaches, processes, and controlling factors. Science of the Total Environment, 838, 156021. https://doi.org/10.1016/j.scitotenv.2022.156021.

Zhang X., Srinivasan R., Hao F., 2007. Predicting hydrologic response to climate change in the Luohe River basin using the SWAT model. Transactions of the ASABE, 50(3), 901–910. https://doi.org/10.13031/2013.23154.

Zhao Q., Liu S., Deng L., Dong S., 2013. Evaluating influences of the Manwan Dam and climate variability on the hydrology of the Lancang-Mekong River, Yunnan Province, southwest China. Journal of Hydrologic Engineering, 18(10), 1322–1330. https://doi.org/10.1061/(ASCE)HE.1943-5584.0000739.